BALLOON MEASUREMENTS OF THE ENERGY SPECTRUM OF COSMIC ELECTRONS BETWEEN 1 GeV AND 25 GeV

James A. Earl, Dennis E. Neely and Thomas A. Rygg

University of Maryland
Department of Physics and Astronomy

Technical Report Number 72-038

September 1971

UNIVERSITY OF MARYLAND
DEPARTMENT OF PHYSICS AND ASTRONOMY
COLLEGE PARK, MARYLAND

Space Physics Group

BALLOON MEASUREMENTS OF THE ENERGY SPECTRUM OF COSMIC ELECTRONS BETWEEN 1 GeV AND 25 GeV* †

James A. Earl, Dennis E. Neely and Thomas A. Rygg

University of Maryland
Department of Physics and Astronomy

Technical Report Number 72-038

* This research was supported in part by the Office of Naval Research contract Nonr-710(19) at the University of Minnesota and by the National Aeronautics and Space Administration grant NGR 21-002-066 at the University of Maryland. Some computer time was provided by NASA Grant NsG-398 at Maryland.

† Revised version

NGR-21-002-068

BALLOON MEASUREMENTS OF THE ENERGY SPECTRUM OF COSMIC ELECTRONS BETWEEN 1 GeV AND 25 GeV

by

James A. Earl, Dennis E. Neely and Thomas A. Rygg
Department of Physics and Astronomy, University of Maryland

ABSTRACT

During three balloon flights made in 1966 and 1967, cosmic electrons were investigated with the aid of a hodoscope detector which provided extensive and detailed information on each cosmic ray event triggering the apparatus. Similar information obtained during calibration exposures to protons and pions as well as to electrons was used to provide identification of cosmic electrons and to determine their energies. Differential primary electron intensities measured in the range from 1 GeV to 25 GeV were substantially larger than some earlier measurements. Taken in conjunction with existing measurements at energies above 100 GeV, this indicates that the energy spectrum of cosmic electrons is steeper than that of cosmic-ray nuclei and, consequently, suggests that Compton/synchrotron energy loss plays a significant role in shaping the electron spectrum.

INTRODUCTION

Today, twelve years after the discovery of electrons among the primary cosmic-rays, there exists no experimental consensus on their energy spectrum. On the one hand, results obtained by Anand, Daniel and Stephens (1968 , 1969) which suggest a power law spectrum having nearly the same slope below 300 GeV as that of the nuclear component, lead to an interpretation in which the age of cosmic electrons is less than 10^6 years,substantially smaller than the value of 3×10^6 years obtained for nuclei from the relative abundances of light and medium nuclei (Shapiro and Silberberg, 1969). On the other hand, independent measurements by Marar, Freier, and Waddington (1971), and by Nishimura, Mikumo, Mito, Niu, Ohta and Taura (1969) give a

relatively small flux at high electron energies and suggest a steep spectrum which would indicate a substantial effect resulting from the Compton/synchrotron mechanism of energy loss acting on electrons over times comparable to or larger than 3×10^6 years. Because the electron spectrum provides information on these and other important astrophysical issues, the resolution of the presently confused situation is an urgent matter.

This paper presents experimental results on the electron spectrum obtained with the aid of a detector whose response to both electrons and nuclei was specified in accelerator exposures carried out in support of balloon exposures to primary cosmic-rays. The instrument provided very complete information on each triggering event. Eight pulse heights were measured and trajectories were defined by a 54 element Geiger tube hodoscope. Because the discrepancies among existing experiments are almost certainly due, in part, to instrumental effects, the procedures that we used to identify electrons, to determine their energies, and to specify their intensities are described in detail so as to allow the reader to form his own opinion of their validity.

APPARATUS AND BALLOON FLIGHTS

The hodoscope is shown in Figure 1. Six crossed trays of Geiger tubes gave a crude stereoscopic description of particle trajectories, served as a guard element able to identify multiple incident particles, and provided information on the number of particles emerging downward from the absorber in association with electromagnetic cascades or nuclear interactions. Each tray contained 9 tubes of 1.58 cm outside diameter and 14.2 cm sensitive length.

Triggering particles were selected by coincidence requirements among tubes in the top four trays chosen so as to define straight line trajectories passing completely through all absorbers and exiting through Tray 6 (see Figure 1). This was accomplished by combining a selected set of eleven two-fold coincidences between tubes in Trays 1 and 3 with a similar set of eleven coincidences based on discharges in Trays 2 and 4. Thus, a group of 121 four-fold coincidences defined incident trajectories suitable for analysis while discriminating against trajectories not suited to unambiguous interpretation. We refer to this scheme as the directional filter.

Although standard mathematical expressions for geometric factors were

not directly applicable, it was possible to group the 121 elementary telescopes (each of which may be visualized as being made up of two square planar elements whose side is equal to one tube diameter) in such a way as to make use of the formulas presented by Critchfield, Ney and Oleksa (1952). Geometric factors so derived are presented in Table I which also contains information on the three balloon flights. Flights 1174 and 1195 were launched from Ft. Churchill, Manitoba and drifted west at ceiling toward a recovery area near Uranium City, Saskatchewan. Flight 1058, which was launched from Minneapolis, Minnesota and recovered near Spooner, Wisconsin, took place on September7, 1966 during a period of enhanced geomagnetic and solar activity following the August 30-September 1,1966 solar event. A temperature compensated Olland cycle pressure transducer was used to measure pressure altitudes at ceiling to an accuracy of $\pm$ 0.2 g/cm^2. The experimental apparatus was destroyed at the end of Flight 1195, but, fortunately, good data had been recorded throughout that flight and accelerator calibrations had been performed. Subsequently, the instrument was reconstructed for further electron calibrations. Details on the format in which information was telemetered and analyzed and on the methods used to determine the sensitive times presented in Table I are given in reports by Neely (1968) and Rygg (1970).

Corrections were applied to take into account, first, acceptable particles rejected because of multiple discharges in one or more of the directional filter trays and, second, acceptable particles which failed to discharge one of those trays because of inefficiency, dead time or leakage between the sensitive volumes of adjacent tubes. The multiple discharge events are due to three distinct phenomena: (1) single inclined trajectories passing through two adjacent tubes, (2) extra discharges caused by knock-on electrons and (3) an effect specific to electrons in which extra discharges, presumably caused by backscattered shower particles, occur in trays immediately above absorbers of high atomic number. Since knock-ons remain close to the primary trajectory and have relatively little penetration power and since the geometric effect involves adjacent tubes by definition, almost all multiple discharges associated with these phenomena involve adjacent tubes. This fact, along with other information about multiple discharges and inefficiency, was verified through an analysis of flight events recorded by a second hodoscope having six trays of counters

in addition to the directional filter instead of only two. Since the second instrument was similar in geometry and arrangement of absorber to the present hodoscope, extensive results obtained through sixfold sampling of each trajectory which passed through the lower trays are directly applicable here. Some of these results are shown in Figure 2 where the probability that a particle will discharge adjacent tubes in passing through a tray is plotted as a function of Z^2, where Z is the charge of the incident particle as determined from pulse height information. The probability at "zero charge" extrapolated according to the Z^2 dependence expected for multiple discharges produced by knock-ons is interpreted as the charge independent, geometric effect due to single trajectories which happen to pass through adjacent tubes. In this way, the multiple discharge probability per tray due to the first two effects was evaluated for minimum ionizing particles as $(1.36 \pm .06)\%$ of which $(.87 \pm .10)\%$ was the geometric effect.

To exhibit the third effect specific to electrons, a detailed breakdown of probabilities for various combinations of discharges in the directional filter observed during electron calibrations from 0.1 GeV to 8.2 GeV is presented in Table II. Of the events having multiple discharges in the directional filter, only 4% are attributed to the knock-on and geometric effects. This figure is less than that derived for flight events because of the smaller geometric effect associated with the collimated accelerator beam. Most of the multiple discharge events are characterized by two discharges in one or more trays and, as is shown in the lower part of the table, these extra discharges occur preferentially in Trays 3 and 4, which are the two trays nearest to the CsI in Counter 3. Since these trays are effectively shielded by Trays 1 and 2, which do not show much of an effect, this observation rules out the possibility that the extra discharges were caused by particles other than the incident electron coming from outside the instrument and suggests that the observed phenomenon is due to low energy shower electrons backscattered within the high Z absorber of Counter 3. Although the relative absence of extra discharges in Trays 1 and 2 may be due, in part, to the greater distance of these trays from the "source" of backscattered particles, there is a strong indication of rapid absorption in the relatively low Z material of the directional filter. This implies that, in future experiments, the importance of backscattering might be significantly

reduced by a low Z shield placed between the elements defining the geometry of the incident beam and the calorimeter. The absence of a strong dependence of the backscattering phenomenon on incident energy is demonstrated by the fact that corresponding probabilities at widely separated energies agree in full detail except for a slight tendency toward higher multiplicities at the higher energies. This is particularly evident in events having non-adjacent discharges. Although our data indicate that an appreciable fraction (15 to 30%) of electron events exhibit triggering multiplicity, the pronounced and strongly energy dependent backscattering phenomena reported at comparable energies by Muller (1971) were not observed.

The probability that a single particle passes through a tray without discharging any tubes was found to be $(3.0 \pm 0.2)\%$ at ceiling and $(1.5 \pm 0.2)\%$ at sea level. The difference between these values represents the effect of inefficiency due to the dead time of the tubes. This is an important factor at balloon altitudes because of the relatively high counting rates encountered there, but it is almost negligible at sea level where the inefficiency is mainly attributed to insensitive regions between tubes. Since the probability of coincidences between an event and a single uncorrelated discharge can be related to the tray inefficiency due to dead time, the measurements show that the probability of an accidental discharge when six trays are involved is not larger than $(0.9 \pm 0.20)\%$ per event. This estimate was based on measured values of (400 ± 20) μsec for the dead time and (5.0 ± 0.5) μsec for the coincidence resolving time.

The scintillation counters shown in Figure 1 were viewed by 1 1/2 inch diameter Type 6199 photomultipliers through adiabatic light pipes coupled to one edge of the phosphor slabs. Separate pulse height analyzers provided independent measurements of the pulse heights in each of the eight counters. These analyzers had a dynamic range of 100 spanned in 16 logarithmic channels each of which covered a factor of 4/3 in pulse height. (Note that $(4/3)^8=10$).

Each of the eight scintillation counters played a specific role which depended upon its position relative to the lead absorber. Counters 1 and 2, which consisted of 15 cm x 15 cm x 0.63 cm sheets of plastic fluor sandwiched among trays of the directional filter, gave two redundant estimates of the ionization rate (dE/dx) of incident particles which were averaged to give a mean value having improved statistical accuracy.

Counter 3, which was placed just below the directional filter and which constituted the first element of the calorimeter, was a 15 cm x 15 cm x 1.89 cm layer of cesium iodide - a scintillation phosphor whose relatively high atomic number provided a thickness of 1.08 radiation lengths in which took place the early stages of shower development, which are of critical importance in identifying electrons. Counters 4 through 8 were 0.63 cm plastic sheets sandwiched among lead absorbers to form, with Counter 3, a calorimeter in which the ionization deposited by shower events could be sampled at the absorber depths indicated at the top of Figure 4.

Scintillation counter sensitivities were evaluated in terms of pulse height spectra for events characterized by a single discharge in each of the six trays - a signature specific to single non-interacting particles penetrating all absorbers and, consequently, having ionization close to minimum ($v/c > .62$). Examples of such distributions recorded during a flight are shown in Figure 3 along with those obtained during a calibration exposure to a mixed beam of protons and pions. To avoid errors from the nuclear interaction "tail" evident in Figure 3, the average pulse height for singly charged minimum ionizing particles was evaluated by fitting a gaussian curve, whose standardized shape was derived for each counter from pre and post flight meson calibration runs, to the peaks of pulse height distributions tabulated at frequent intervals during flights. This procedure eliminated instrumental drifts in average pulse height larger than 0.2 channels or 5.9%. The r.m.s. width of the minimum ionization pulse height distributions was typically $\pm$ 1.3 channels ($\pm$ 45%) for the plastic counters and $\pm$ 1.0 channel ($\pm$ 33%) for Counter 3.

A potentially important consideration in the correct interpretation of events produced by high energy electrons is the saturation of photomultiplier output currents arising from space charge limiting. This phenomenon leads to underestimation of large pulse heights and, hence, to a corresponding underestimate of the energy content of large showers. Such effects were investigated by comparing output signals from two photomultipliers operating with flight electronics and viewing simultaneously light pulses generated by sea level cosmic ray events in a thick slab of plastic scintillator placed between trays of a directional filter. Because of improved light collection and increased thickness of the slab, the pulses obtained from single mesons

selected by the directional filter were many times larger than corresponding pulses from the flight scintillators while occasional pulses from events of high multiplicity fell well above the largest pulse height that could be measured by the analyzers in their flight configuration. To make evident saturation effects occuring in this region of large pulse heights, one tube was operated at reduced voltage, a step which reduced both the gain and the importance of saturation at a given light input, while the other tube was operated with full voltage but with an attenuator in its output circuit, a step which reduced the gain without affecting the saturation. In this modified configuration, limiting would appear as a systematic deviation from proportionality in the relationship between the pulse heights from the two multipliers. The fact that such deviations were not observed shows that saturation had a negligible effect on pulses up to five times larger than the maximum recorded during flights. The absence of saturation was also confirmed by the fact that the pulse height distributions for all events triggering during flights exhibited a constant logarithmic slope at large pulse heights and did not show any signs of the cut-off or increase in slope expected in the presence of limiting.

CALIBRATION PROCEDURES AND IDENTIFICATION OF ELECTRON EVENTS

The fact that only a few percent of the primary cosmic rays are electrons imposes severe demands upon the techniques used to distinguish true electron events from an inevitable background of superficially similar events produced by the nucleonic component. This problem has been solved through detailed knowledge of shower electron trajectories obtained with cloud chambers (Earl, 1961) with nuclear emulsions (Daniel and Stephens, 1965; Freier and Waddington, 1965; Marar, Freier, and Waddington, 1971; Nishimura, et al., 1969) and with spark chambers (Agrinier, Koechlin, Parlier, Boella, Degli, Antoni, Dilworth, Scarsi, and Sironi, 1964; De Shong, Hildebrand, and Meyer, 1964; Oran, Frye, and Wang, 1969) through the use of gas Cerenkov counters (Webber and Chotkowski, 1967; L'Heureux and Meyer, 1965) and through the use of subtraction procedures based on the differing characteristics of shower development in materials of different atomic numbers (Bleeker, Burger, Scheepmaker, Swanenburg, and Tanaka, 1966; Rubstov, 1966). The present experiment takes advantage of a technique in which shower development is sampled throughout a thick high Z absorber in order to identify electron events through the more rapid growth and decay of electromagnetic showers compared to nuclear cascades. In applying this technique, use was made of detailed empirical knowledge of both electron and nuclear events obtained in calibration exposures made at the 2 GeV and 10 GeV electron synchrotrons at Cornell University and at the 28 GeV Alternating Gradient Synchrotron (AGS) at Brookhaven National Laboratory. The method yields a statistical identification in which electron events are exhibited as a peak resolved from the nuclear background, but identification of individual events was not achieved.

The basic data derived from the electron calibrations were a set of shower curves for several incident electron energies giving ionization, expressed in terms of the average scintillation counter pulse height for minimum ionizing particles, as a function of depth in the absorber.

In an earlier version of this paper (Neely, 1968), calibration exposures had been made only in the energy range from 0.1 GeV to 1.2 GeV and, consequently, it was necessary to derive from these low energy data shower curves applicable at higher energies. Such curves were constructed by using

Approximation B of shower theory (Rossi 1952) as an extrapolation formula with the radiation length and critical energy treated as variables which were adjusted to produce good agreement between measured and calculated curves at 1.0 GeV. Recently, a rebuilt version of the apparatus essentially identical to that flown was exposed to electrons with energies up to 8.2 GeV. The new calibration data (1971 exposure) were in good agreement not only with the earlier data (1967 exposure) in a region of overlap at low energies but also with the extrapolated results deduced at higher energies. This agreement gives empirical verification of the shower curves used to analyze cosmic electrons from 1 GeV to 8.2 GeV and provides a basis for the relatively minor extrapolations involved in extending the spectral measurements to 25 GeV.

Calibration data are summarized in Figure 4, where the shower profiles used in the analysis of flight data are shown by solid curves calculated as described above for a logarithmic sequence of electron energies spaced by a factor of 1.78. Also indicated at the the top of Figure 4 are the absorber thicknesses in radiation lengths above each counter and each tray. Note that the thicknesses used during Flights 1174 and 1058 were identical but somewhat less than those of Flight 1195. The observations and calculated curves of Figure 4 are in only fair agreement with the Monte Carlo calculations of Nagel (1965) which predict, for shower electrons above 1.5 MeV, about 20% more particles than are observed at maximum and about half as many as are observed in the region of exponential absorption at large depths. Because of the inherent complexity of shower phenomena the discrepancy between observations and Monte Carlo calculations is not disturbing especially when the enhanced ionization of non-relativistic particles below the cut-off energy of the calculations and the significant response of plastic scintillators to the low energy photons abundant in showers are taken into consideration.

The apparatus and analysis procedures are such that measured electron energies are relatively insensitive to details of the shower curves, for the energy content of events is essentially specified in terms of observed track length independent of the distribution in depth. In this sense, the instrument behaves as an ionization calorimeter. Errors in the shower curves can, of course, lead to increased uncertainty in the identification of electrons

because of poor agreement between observed and assumed shower profiles. However, this is not of great significance, because, as will be demonstrated later, the nuclear background is of relatively minor importance at high energies where the shower curves are most uncertain. Calorimetric energy measurements are characterized by the ratio of incident energy to track length, a parameter whose value was defined in the course of the calibration experiments as 17.8 ± 1.5 MeV/rl integrated over all depths. Throughout this paper the radiation length in lead is taken to be 5.82 g/cm^2.

The identification of electrons was based on a comparison of the electron shower curves of Figure 4 with ionization vs. depth profiles recorded during flights by Counters 3 through 8 for triggering events which satisfied certain acceptance criteria. Better agreement with the shower curves is obtained, on the average, for electrons than for nuclear events. The comparison was carried out in terms of a parameter S defined as:

$$S = \frac{1}{6} \sum_{\text{Counter 3}}^{\text{Counter 8}} \frac{(\text{Pulse Height Observed} - \text{Pulse Height Expected})^2}{(\text{Standard Deviation of Expected Pulse Height})^2}$$

in exactly the same way as the familiar statistical χ^2 parameter. For each event the nominal electron energy, which determines the expected pulse heights and standard deviations, was varied until a minimum value S_{min} was found. In this way each event was assigned a nominal energy E_{nom} and a parameter S_{min} measuring the degree to which the event fit an electron shower curve of energy E_{nom}.

Typical distributions of S_{min} obtained when this procedure was applied to events produced by accelerator electrons are shown in Figure 5. At energies below 3.2 GeV, good agreement was obtained with the χ^2 distribution for five degrees of freedom which is expected, a priori, on the basis of the exact analogy between the definitions of S and χ^2. (Only five degrees of freedom are involved in fitting to six pulse heights because the minimization procedure effectively "removes" one degree of freedom). Above 3.2 GeV, the observed distribution is shifted relative to the χ^2 curve toward smaller values of S_{min}. We believe that this shift was caused by the distinctly skewed pulse height distributions observed in some counters at high energies. These violate the Gaussian assumption basic to the χ^2 treatment and result in standard deviations which are, in effect, too large. In any case, the fact

that a well defined electron "peak" in the S_{min} distribution persists over a wide range of energies provides a powerful tool for resolving electrons.

The distribution of E_{nom} obtained by applying the above minimization procedure to accelerator electrons of fixed incident energy is, in effect, the energy resolution function of the experiment. Such distributions, shown in Figure 6, exhibit a fractional width of $\pm$ 50% at 1 GeV improving to $\pm$ 30% at 8.2 GeV.

Two criteria were used to select for detailed analysis a sample of flight events rich in energetic electrons. First, the ionization rate of incident particles as measured in Counters 1 and 2 was required to be less than 2.5 times minimum, a value chosen so as to ensure optimum separation between electrons and helium nuclei. A second criterion, which tended to select events in which many particles emerged from the lead absorber, was based on tube discharges in trays 5 and 6; exactly two discharges in each tray or more than two discharges in either tray were required. This criterion was needed to discriminate against penetrating protons, a small fraction of which generate ionization profiles similar enough to the profiles of electrons to cause confusion when the protons are overwhelmingly more numerous. Since the probability of multiple knock-ons is very small, events satisfying the second criterion will be designated as "interacting" while those that penetrate to trays 5 and 6 with low multiplicity will be called "non-interacting."

Although the multiplicity criterion greatly increases the ratio of electrons to protons among the events it selects, it unavoidably introduces an energy dependent bias in the selection of electrons. Selection probabilities, as presented in Figure 7, exhibit a strong bias against electrons below 2 - 5 GeV but give nearly unbiased selection above 6 - 8 GeV.

The effectiveness of the minimization procedure and selection criteria described above was tested with nuclear events recorded at the Brookhaven AGS accelerator in a calibration beam of positive charge and known momentum but containing an unspecified mixture of protons and pions. Since we are concerned with characteristics of nuclear interactions in lead which are not very dependent on the nature of the incident particle, this ambiguity in composition is not thought to be a serious shortcoming. Events recorded

with and without a 3 radiation length lead plate placed just in front of the directional filter were used to rule out the presence of any significant flux of electrons in the calibration beam. Data were recorded at rigidities of 0.4, 0.6, 2.0, and 4.0 GV. Because the characteristics of events produced by protons and pions were relatively independent of incident energy in comparison to those produced by electrons, we will concentrate on data taken at 4.0 GeV which have the best statistics and are most typical of primary cosmic rays.

The χ^2 curve, typical of the S_{min} distributions for electrons, is compared in Figure 8 with empirical distributions obtained for nuclear events recorded at Brookhaven. It will be noted that the peak for interacting protons and pions is about a factor of five smaller than the electron peak and is shifted toward much larger values of S_{min} ($S_{min} \gtrsim 8$). This relationship results in a proton rejection ratio of 100:1 at the peak of the electron curve ($S_{min} = 1.0$) improving to 400:1 in the region $S_{min} < 0.5$. These ratios refer to a sum over all nominal energies. Since the nominal energies of nuclear events are predominantly below 1 GeV, the rejection ratios for events of high nominal energy are even higher. The fact that the peak for "non-interacting" particles lies relatively close to the electron curve leads to great difficulties in distinguishing these events from electrons and points up the advantage of having trajectory information which makes possible a separation based on multiplicity.

Data from Flight 1058 treated in the same way as the calibration data are summarized in Figure 9. Interacting events were categorized according to whether their nominal energy was greater than or less than 1 GeV. It is apparent that the distribution for $E_{nom} > 1$ GeV is resolved into two components: electrons, represented by the χ^2 curve reproduced as in previous figures, and protons, represented by the dashed curve derived from calibration data for interacting particles of $E_{nom} > 1$ GeV in the same way as the curves of Figure 8. The flight events of nominal energy less than 1 GeV are well represented by the solid calibration curve describing nuclear events. In other words, since the events produced by electrons of energy less than 1 GeV do not satisfy the selection criterion for interacting particles (see Figure 7), an electron contribution below 1 GeV is not expected in Figure 9 and is, in fact, not observed.

In the bottom part of Figure 10, S_{min} distributions similar to those of Figure 9 are presented for interacting events restricted to the band of nominal energies centered at 5.6 GeV (4.2 to 7.5 GeV) and recorded during Flight 1058 (circles) and the Brookhaven calibration (squares). Good separation of protons and electrons is obtained, with a proton rejection ratio greater than 10:1 for $S_{min} < 1$ confirming that the resolution improves as the energy is increased. Note that, in this figure, the two sets of data are plotted on an absolute basis derived from the relative numbers of minimum ionizing non-interacting events observed during calibration and flights. Thus, the agreement exhibited for $S_{min} > 1$ is an indication that the number of events of this nominal energy contributed at large values of S_{min} by 4 GV calibration particles was approximately the same as that contributed by the average cosmic ray. Since it has been demonstrated that the contribution of nuclear particles at 2 and 4 GV for $S_{min} < 1$ is small relative to the number of events observed in that region during flights (see Figures 8,9, and 10), the interpretation of any significant fraction of such flight events as nuclear interactions would imply a radical change in the S_{min} distribution such that the relatively few cosmic rays above 4 GV would contribute orders of magnitude more events to the region $S_{min} <1$ than those below 4 GV. An examination of 2 and 4 GV calibration events, which exhibit a slowly increasing energy dependence of these events, gives no indication of such pronounced variations.

At the top of Figure 10, a normalized distribution obtained by dividing the observed number of particles by the probability calculated from the χ^2 distribution is presented. In this representation, the electron peak appears as a horizontal line at low values of S_{min} while components not following the electron distribution appear as steeply sloping lines. At each energy, the separation between electrons and protons was carried out with the aid of such a normalized curve on which the value of S_{min} where the nuclear contribution dropped to one-tenth that of electrons was estimated. All interacting events with S_{min} below this value were counted as electrons in terms of which the total number of electrons could be determined with the aid of known probabilities derived from Figure 5. In practice, this amounted to taking events below S_{min} of 1.2 (77% of the electrons) and 0.86 (61% of the electrons) for nominal energies above and below 4.2 GeV, respectively.

It has been suggested that secondaries from nuclear interactions produced in the calorimeter by the numerous particles which enter outside of the normal triggering geometry could occasionally satisfy both the triggering and selection criteria and be mistaken for electrons. To check on this possibility, we have plotted in Figure 11 a histogram giving, for Flight 1195 events with $S_{min} < 1$, the number of tube discharges in Tray 6 as a function of horizontal displacement from the axis defined by discharges in the directional filter. These events, most of which were identified as electrons, follow accurately the expected distribution calculated for electrons by folding together the displacement histograms for accelerator electrons and for penetrating particles observed in flight (solid curve). In contrast, for the nuclear events described above, there is no correlation between discharges in the directional filter and those in lower trays, and the expected distribution is that calculated by assuming equal discharge probabilities for each tube in Tray 6 (dashed curve).

RESULTS

The spectrum of cosmic electrons was defined in two steps. First, the spectrum of electrons observed at the balloon was calculated taking into account the effects of finite resolution in energy and of selection bias, as indicated in Figures 6 & 7. Then the observed spectrum was corrected for secondary production and bremsstrahlung energy loss in the residual atmosphere above the balloon.

Because of the rapid variation with energy of the spectral intensity, which is implied not only by the power law character of the primary spectrum but also by the pronounced energy dependence of the selection probability, the dispersion in nominal energies assigned to events produced by electrons of a fixed incident energy can lead to significant errors if not taken into consideration. To compensate for this effect, we used a matrix inversion method in which a set of linear equations expressing the number of particles observed in each energy interval in terms of integrals involving the spectrum and resolution function of Figure 6 was solved to yield corrected estimates of the spectral intensities. The justification for applying the resolution correction before taking into account the effect of selection probability is that correlations between numbers of shower particles observed at different

depths are small (Brecht 1969). Hence, the use of a multiplicity criterion based on discharges in trays separated in depth from all counters has essentially no effect on the nominal energies of events so selected.

In Figure 12, spectra observed at the balloon during Flight 1195 (Churchill, 2.0 g/cm^2) and Flight 1058 (Minneapolis, 8.3g/cm^2) are presented. Although the lowest energy point for Flight 1058 was below the nominal geomagnetic cutoff of 1.3 GV (Shea, Smart, and McCracken, 1965), the observed flux of helium nuclei stopping in Counter 3 indicated that the full intensity of primary helium was present above 0.9 GV. Thus, since a depression of geomagnetic cutoffs similar to those reported for other disturbed periods (Winckler, Bhavsaar, and Peterson, 1961) appears to have been present during Flight 1058, electrons between 0.9 GeV and 1.3 GeV incident during that flight were interpreted as primaries rather than as reentrant albedo. Each point plotted in Figure 12 represents the differential intensity at the center of a logarithmic energy interval spanning a factor of 1.78, with squares and circles representing, respectively, the spectra before and after correction for selection effects. Above 5 GeV, where the selection probability is very nearly equal to one, these spectra merge. At low energies, the fact that the absorber thicknesses were not the same for the two flights led to significant differences between the spectra observed before correction for selection bias. After corrections based on the probabilities of Figure 7 were applied, the selection effects at low energies disappeared leaving the spectrum of Flight 1195 systematically higher by about a factor of 1.4 over the entire range from 1 GeV to 10 GeV. Although solar modulation and atmospheric secondaries may play a minor role in producing this difference, we think that it is best interpreted as an effect due to bremmstrahlung energy loss in the air above the balloon. Because the electron spectrum is quite steep, even the relatively small energy losses occuring at balloon altitudes can have significant effects on the observed spectrum.

Since the average energy of electrons subject to bremstrahlung decreases exponentially with an e-folding distance of one radiation length (37.7 g/cm^2 in air), energy losses can be taken into account by multiplying all energies measured at the balloon by a factor exp ($+$ X/37.7) which depends only on the depth X. This has the effect of shifting each point on a differential energy spectrum upward in energy and downward in intensity

by the same factor. On a typical log-log plot, the points are displaced diagonally downward to the right. Although this procedure is relatively insensitive to spectral shape, it is strictly correct only for power law spectra. A more elaborate procedure taking into account fluctuations in radiation loss is called for in dealing precisely with spectra of rapidly changing slope, but these refinements are not appropriate here. For a power law spectrum with index γ, these considerations lead to a differential intensity at a fixed energy which depends on depth as $\exp-\{(\gamma-1)\cdot(x/37.7)\}$.

On the grounds that photons produced in the 5.7 g/cm^2 of material in the directional filter would almost always enter the calorimeter where their energy would be correctly added to the residual energy of the incident electron, no corrections were applied for bremmstrahlung in the instrument itself. In any case, the fact that calibrations and flights were carried out with the same amount of material above the calorimeter ensured correct assignment of energies.

In Figure 13 and Table III are presented primary electron spectra at the top of the atmosphere corrected for bremmstrahlung as indicated above and for atmospheric secondary electrons using the calculations of Beuermann (1971). However, the contribution of secondaries was appreciable only in the two lowest energy intervals where it was comparable to statistical uncertainties. The agreement among the three sets of data presented in Figure 13 is remarkable, especially in view of the marked deviations evident in Figure 12. The fact that significantly different experimental configurations flown at different depths yield identical results is, in itself, evidence that electrons were correctly identified.

DISCUSSION

Marar, Freier, and Waddington (1971) have summarized the extensive literature on cosmic electron experiments and have called attention to the existence of marked discrepancies among independent spectral measurements. There is no point in repeating their compilation here. Published information provides little or no basis for reconciling the discrepancies. Under these circumstances, we are forced to trust our own data and discuss their implications with only enough intercomparison with other experiments to lend perspective. In this spirit, we note that the intensities of Table III are

among the highest reported. They are in very good agreement with the satellite observations of Marsden, Jakeways, Crowden, Napier, and Calder (1969) and of Bleeker, Burger, Deerenberg, Van de Hulst, Scheepmaker, Swanenburg, and Tanaka (1969) and in fair agreement with balloon observations of Fanselow, Hartman, Hildebrand, and Meyer (1969), but they are significantly larger than the rest of the measurements tabulated by Marar et al. Relatively high electron intensities are indicated by observations of cosmic radio noise (Alexander, Brown, Clark, Stone, and Weber, 1969) and are consistent with a detailed reconciliation of radio and cosmic ray observations carried out by Goldstein, Ramaty, and Fisk (1970). The latter have also shown that solar modulation is negligible above 5 GeV where the differential fluxes of Figure 13 can be represented by the power law:

$$\frac{dJ}{dE} = 1000 \quad E^{-3.3 \pm 0.1} \text{ particles/m}^2\text{sec sterad GeV}$$

where E is expressed in GeV. This expression characterizes the interstellar spectrum of cosmic electrons as determined by this experiment.

Although there is no proof of the assumption that the slope of the electron spectrum unmodified by Compton-synchrotron losses is identical to that of the nucleonic spectrum, any interpretation of the fact that the above spectral index is larger than the nucleonic value of 2.6 in terms of this plausible hypothesis leads to the conclusion that energy loss processes play a significant role in steepening the observed electron spectrum. In the classical theory of Compton/synchrotron steepening (Tunmer, 1959), the electron spectrum is characterized by a break energy E given, in GeV, by the expression:

$$\text{WET} = 307$$

where W is the total electromagnetic energy density in eV/cm^3 and T is the average electron exposure time in millions of years (Myr.). If we adopt 5 GeV as an upper limit on the break energy imposed by the onset of modulation, and assume W = 0.92 eV/cc, a value which includes the contributions of the microwave background radiation (0.38 eV/cc), of starlight (0.3 eV/cc) and of a galactic magnetic field of 3×10^{-6} gauss (0.24 eV/cc), then the exposure time must be greater than 66 Myr. If the

intense infrared radiation reported by Shivanandan, Houck, and Harwit (1968) exists (W = 14 eV/cc), then an exposure time greater than 4.4 Myr is required. This value agrees with the conventional "age" of cosmic rays deduced from the abundances of L_i, B_e and B (Shapiro and Silberberg 1969). However, the presence of an intense infrared component is not consistent with upper limits set by observations of interstellar molecular absorption (Bortolot, Clauser, and Thaddeus 1969).

To confirm the steepening discussed above, we have compared, in Figure 14, our results with observations of electrons above 100 GeV (Nishimura, Mikumo, Mito, Niu, Ohta, and Taira 1969) (Anand, Daniel, and Stephens 1969) (Marar, Freier, and Waddington, 1971). (The use as ordinate of differential intensities multiplied by E^3 has the effect of mapping a steeply sloping cosmic ray energy spectrum into a slowly varying function of E and of making more evident any discrepancies between data points or changes in spectral steepness.) The solid line which describes the power law given earlier extrapolates rather well through the measurements of Nishimura et al. and of Marar et al. On the other hand, the dashed curve, $dJ/dE = 480\ E^{-3}$, also agrees with our points and those of Anand et al. In either case an electron spectrum significantly steeper than the nucleonic spectrum is suggested.

The data of Figure 14, as well as preliminary results of Silverberg, Ormes, Balasubrahmanyan and Ryan (1971), suggest spectral indices in the range from 3.0 to 3.5 which are a little smaller than the classic steepening by one power of E but which agree with the spectrum calculated by Jokipii and Meyer (1969). This calculation, in which electrons produced in the galactic disc diffuse within an infinite isotropic medium, predicts two characteristic energies bounding a region of spectral slope steepened by one half power of E. The smaller of these energies, which must be identified with the 5 GeV upper limit discussed above, corresponds to the characteristic time for spherical diffusion over a region of galactic radius. The lower limit of 66 Myr, now applicable to this time, is consistent, within the framework of the model, with the Li Be B age of nucleonic cosmic rays because fragmentation occurs only during the small fraction of the time spent by cosmic rays in the galactic disc. Although confirmation of this specific model will require more evidence than the exhibition of a power law

electron spectrum of appropriate slope, such a spectrum would indicate the validity of the essential feature of the model, which is diffusive propagation of electrons from a localized source region.

ACKNOWLEDGEMENTS

This project was begun under Office of Naval Research contract Nonr-710 (19) at the University of Minnesota where Charles W. Carlson and Steven C. Gustafson played an important role in the early development of the instrument. At Maryland, support has been provided by National Aeronautics and Space Administration Grant NGR 21-002-066. Some computer time was provided by NASA Grant NsG-398 through the Computer Science Center at the University of Maryland. In carrying out calibrations, invaluable aid was provided at Cornell by Drs. Berkelman, Nordberg, Mistry, Rouse, DeWire and McDaniel and at Brookhaven by Mr. Bill Walker. Balloon flights were carried out under the Office of Naval Research Skyhook Program. The assistance of H. Demoski and M.O. Evanick in arranging for flights is gratefully acknowledged.

REFERENCES

Agrinier, B., Y. Koechlin, B. Parlier, J. Basseur, C. J. Bland, G. Boella, C. Dilworth, L. Scarsi, and G. Sironi, Flux of primary cosmic-ray electrons of rigidity above 4.5 BV., *Phys. Rev. Letters, 13,* 377,1964.

Alexander, J. K., L. W. Brown, T. A. Clark, R. G. Stone, and R. R. Weber, Low frequency cosmic noise observations of the constitution of the local system, *Astrophys. J. Letters, 157,* L163, 1969.

Anand, K. C., R. R. Daniel, and S. A. Stephens, Cosmic-ray electron spectrum above 50 BeV and its implications for cosmic-ray confinment, *Phys. Rev. Letters, 20,* 764, 1968.

Anand, K. C., R. R. Daniel, and S. A. Stephens, The cosmic-ray electron spectrum at energies > 100 GeV, *Proc. of the Eleventh Intern. Conf. on Cosmic Rays,* Budapest, 1969.

Beuerman, K. P., Secondary electrons and photons in the upper atmosphere, *J. Geophys. Res., 76,* 4291, 1971.

Bleeker, J. A. M., J. J. Burger, A. Scheepmaker, B. N. Swanenburg, and Y. Tanaka, A balloon observation of high energy electrons, *Proc. of the Ninth Intern. Conf. on Cosmic Rays, London, Vol. 1,* 327, 1965.

Bleeker, J. A. M., J. J. Burger, A. J. M. Deerenberg, H. C. Van de Hulst, A. Scheepmaker, B. N. Swanenburg, and Y. Tanaka, The cosmic ray electron spectrum between 0.5 and 10 GeV observed on board OGO-5, *Proc. of the Eleventh Intern. Conf. on Cosmic Rays,* Budapest, 1969.

Bortolot, V. J., J. F. Clauser, and P. Thaddeus, Upper limits to the intensity of background radiation at λ = 1.32, 0.559, and 0.359 mm, *Phys. Rev. Letters, 22,* 307, 1969.

Brecht, J. J., An experimental investigation of fluctuations and correlations in electromagnetic and nuclear showers developing in lead, M. S. Thesis, *Univ. of Maryland Tech. Rept. 955,* 1969.

Critchfield, C. L., E. P. Ney, and S. Oleksa, Soft radiation at balloon altitudes, *Phys. Rev., 85,* 461, 1952.

DeShong, J. A., R. H. Hildebrand, and P. Meyer, The ratio of electrons to positrons in the primary cosmic rays, *Phys. Rev. Letters, 12,* 3, 1964.

Earl, J. A., Cloud chamber observations of primary cosmic ray electrons, *Phys. Rev. Letters, 6,* 125, 1961.

Fanselow, J. L., R. C. Hartman, R. H. Hildebrand, and P. Meyer, Charge composition and energy spectrum of primary cosmic-ray electrons, *Astrophys. J.*, *158*, 771, 1969.

Freier, P. S., and C. J. Waddington, Singly and doubly charged particles in the primary cosmic radiation, *J. Geophys. Res.*, *70*,5753, 1965.

Goldstein, M. L., R. Ramaty, and L. A. Fisk, Interstellar cosmic ray spectra from the nonthermal radio background from 0.4 to 400 MHz, *Phys. Rev. Letters*, *24*, 1193, 1970.

Jokipii, J. R., and P. Meyer, Storage and diffusion of cosmic-ray electrons in the galaxy, *Phys. Rev. Letters*, *20*, 752, 1968.

L'Heureux, J., and P. Meyer, Flux and energy spectrum of primary cosmic ray electrons, *Phys. Rev. Letters*, *15*, 93, 1965.

Marar, T. M., P. S. Freier, and C. J. Waddington, Intensity and energy spectrum of energetic cosmic ray electrons, *J. Geophys. Res.*, *76*, 1625, 1971.

Marsden, P. L., R. Jakeways, J. B. Crowden, T. M. Napier, and I. R. Calder, High energy electrons recorded on the ERSO II satellite, *Proc. of the Eleventh Intern. Conf. on Cosmic Rays*, Budapest, 1969.

Muller, D., Measurement of the cosmic ray electron spectrum at very high energies, *Bul. Am. Phys. Soc.*, *16*, 654, 1971.

Nagel, H. H., Elektron-photon kaskaden in blei, *Z. Phys.*, *186*, 319, 1965.

Neely, D. E., A cosmic electron detector, M. S. Thesis, *Univ. of Maryland Tech. Rept. 845*, 1968.

Nishimura, J.,E. Mikumo, I. Mito, K. Niu, I. Ohta, and T Taira, The observation of electron component in cosmic rays with emulsion chamber, *Proc. of the Eleventh Intern. Conf. on Cosmic Rays*, Budapest, 1969.

Oran, W. A., G. M. Frye, and C. P. Wang, Flux and energy spectrum of cosmic ray electrons at 42° north geomagnetic latitude in October 1967, *J. Geophys. Res.*, *74*, 53, 1969.

Rossi, B., *High Energy Particles*, Prentice Hall Inc., Englewood Cliffs, New Jersey, 1952.

Rubstov, V. I., Measurements of cosmic ray electron intensity, *Proc. of the Ninth Intern. Conf. on Cosmic Rays, London, Vol. 1*, 324, 1966.

Rygg, T. A., Cosmic ray proton and helium measurements over half a solar cycle 1965-1969, M. S. Thesis, *Univ. of Maryland Tech. Rept. 70-111*,1970.

Shapiro, M. M., and R. Silberberg, Lifetime of cosmic rays, *Proc. of the Eleventh Intern. Conf. on Cosmic Rays*, Budapest, 1969.

Shea, M. F., D. F. Smart, and K. G. McCracken, A study of vertical cutoff rigidities using sixth degree simulations of the geomagnetic field, *J. Geophys. Res.*, *70*, 4117, 1965.

Shivanandan, K., J. R. Houck, and M. O. Harwit, Preliminary observations of the far-infrared night-sky background, *Phys. Rev. Letters*, *21*, 1460, 1968.

Silverberg, R. F., J. F. Ormes, V. K. Balasubrahmanyan, and M. J. Ryan, The primary cosmic ray electron spectrum from 10 GeV to about 200 GeV, *Proc. of the Twelfth Intern. Conf. on Cosmic Rays*, Tasmania, 1971.

Tunmer, H., The relation of cosmic radio emission to the electronic component of cosmic rays, *Mon. Not. Roy. Astron. Soc.*, *119*, 184, 1959.

Webber, W. R., and C. Chotkowski, A determination of the energy spectrum of extraterrestrial electrons in the energy range 70 - 2000 MeV, *J. Geophys. Res.*, *72*, 2783, 1967.

Winckler, J. R., P. D. Bhavsar, and L. Peterson, Time variations of solar cosmic rays during July 1959 at Minneapolis, *J. Geophys. Res.*, *66*,995, 1961.

Table I

Balloon Flight Summary

Flight No.	1174	1058	1195
Launch Location	Churchill	Minneapolis	Churchill
Ceiling Altitude (g/cm^2)	6.3	8.3	2.0
Reached Ceiling (UT/Date)	1200 July 30, 1966	0230 Sept. 7, 1966	1420 July 12, 1967
Termination (UT/Date)	1510 July 30, 1966	2300 Sept. 7, 1966	0315 July 13,1967
Geometric Factor* (cm^2 sterad)	8.1±0.3	7.4±0.3	7.7±0.3
Average Sensitive Time per event (sec)	.202	.245	.225
Total Number of Usable Events	11,326	56,330	115,829
Total Number of Clean Events**	5,697	26,528	50,963
Total Exposure (m^2 sterad sec)	1.85±.07	10.2±0.5	20.1±0.7
Percent of time at ceiling not spent on usable events	11.4	32	3.7

*All corrections included except for the effect of backscattered shower electrons.

**Clean events are those which trigger without multiple discharges in the directional filter.

Table II

Directional Filter Discharge Probabilities for Electron Events

Percentage probabilities	1967 Calibration .10 GeV	.15 GeV	.30 GeV	.60 GeV	1.0 GeV	1.2 GeV	1971 Calibration 1.0 GeV	1.8 GeV	3.3 GeV	5.6 GeV	8.2 GeV
One and only one discharge in each tray	85±1	83±1	82±1	80±1	81±1	80±1	78±1	76±1	72±1	71±1	71±1
Two adjacent discharges in one or more trays*	10±1	12±1	12±1	12±1	11±1	12±1	14±1	15±1	16±1	16±1	15±1
Two non-adjacent discharges in one or more trays	3.8±0.5	4.0±0.4	5.1±0.6	6.2±0.5	7.1±0.6	6.0±0.4	6.7±0.4	7.3±0.7	10.±0.4	12.±0.5	13.±0.4
More than two discharges in one or more trays	1.0±0.3	0.8±0.2	1.4±0.3	1.1±0.2	1.3±0.3	1.3±0.2	1.5±0.2	1.7±0.3	1.7±0.2	1.4±0.2	1.5±0.2
Events not satisfying directional filter requirement	0.3±0.1	.08±.06	0.8±0.3	0.8±0.2	0.4±0.1	0.2±0.1	---	---	---	---	---
Two adjacent discharges in:											
Tray 1	0.8±0.2	1.3±0.2	1.3±0.2	1.5±0.2	0.9±0.2	1.3±0.2	1.7±0.2	1.2±0.3	1.4±0.2	1.2±0.2	1.1±0.1
2	2.4±0.4	2.0±0.3	2.0±0.4	2.5±0.3	2.5±0.4	2.3±0.2	2.5±0.3	3.0±0.5	3.1±0.2	3.0±0.3	2.9±0.2
3	3.6±0.5	4.3±0.4	5.5±0.6	5.0±0.4	4.7±0.5	5.5±0.3	6.2±0.4	6.0±0.6	6.4±0.3	6.1±0.4	5.4±0.3
4	4.9±0.5	6.8±0.5	5.7±0.7	6.5±0.5	5.4±0.5	6.5±0.4	7.3±0.4	7.9±0.7	8.1±0.4	9.0±0.4	8.0±0.3

*The probability of two adjacent discharges in one or more trays due to knock-ons and multiple penetrations is estimated as 4.0 ± 0.5 %.

Table III

Electron differential intensities corrected to the top of the atmosphere.

Flight No.	Energy* (GeV)	Raw number of Electrons observed	Intensity p/m^2 sec sterad GeV
1174	1.6	2	23 ± 16
	3.7	4	5.6 ± 3.0
	6.6	6	1.7 ± 0.7
	11.8	6	0.65 ± 0.27
	21.0	1	0.05 ± 0.05
1195	1.05	5	58 ± 27
	1.9	6	14 ± 6
	3.3	25	7.8 ± 1.6
	5.9	56	2.7 ± 0.4
	10.5	39	0.47 ± 0.08
	18.8	10	0.057± 0.018
1058	1.25	3	18 ± 16
	2.2	12	10 ± 4
	3.9	37	6.8 ± 1.1
	7.0	21	0.9 ± 0.2
	12.5	17	0.32 ± 0.08
	22.2	4	0.032± 0.016

*Intensities quoted are based on the number of electrons with nominal energies falling in a logarithmic interval spanning the range from 0.75 E_o to 1.33 E_o , where E_o is the energy in this column. However, corrections for the effects of averaging over this finite interval were applied in such a way that differential intensities presented in this table refer to the energy E_o .

FIGURE CAPTIONS

Fig. 1. Cross sectional diagram of the instrument. Trays of Geiger tubes, scintillation counters and lead absorbers all have lateral dimensions of 15 cm × 15 cm.

Fig. 2. Probability that a single particle penetrating a tray of tubes will produce two adjacent discharges.

Fig. 3. Scintillation counter pulse height distributions. Note the alpha particle peak in Channel 9 and the nuclear interaction tail appearing in Counter 6 at large pulse heights. Because it is separated from heavy material and shielded by the directional filter, Counter 2 does not exhibit a tail.

Fig. 4. Shower curves used in this paper to identify electron events. Circles refer to the 1967 calibration. Triangles and squares refer to the 1971 calibrations of the Flight 1058 and 1195 configurations, respectively. These symbols are also used in Figs. 5, 6 and 7. Solid curves were calculated as described in the text. Numbers associated with the curves give electron energies in GeV while the depths of various counters and trays are indicated at the top of the figure.

Fig. 5. Probability distributions for electron events recorded during calibrations. The abscissia is the parameter S_{min} defined in the text. The ordinate gives the probability that an event will fall in a logarithmic interval of S_{min} of width ± 17%. In evaluating the agreement between experimental points and solid theroretical curves, note that no normalization of either abscissa or ordinate was employed.

Fig. 6. Energy resolution functions giving the probability that electron events having energies indicated will be assigned nominal energies above, below or agreeing with the actual energy.

Fig. 7. The selection probability for events satisfying a criterion on the multiplicity of discharges in Trays 5 and 6 is plotted as a function of electron energy.

Fig. 8. Probability distributions, similar to those of Figure 5, for electrons and for protons and pions recorded during the calibration exposure at Brookhaven.

Fig. 9. Probability distributions, similar to those of Figure 5, for interacting events recorded during flights.

Fig. 10. Presented below, are probability distributions, similar to those of Figure 5, for interacting flight events having nominal energies between 4.2 GeV and 7.5 GeV. Above, are probability distributions normalized by dividing the observed probabilities by the probabilities expected for electrons as given by the χ^2 distribution function.

Fig. 11. Observed discharge probability of tubes in Tray 6 as a function of displacement from shower axis for flight electrons agrees with that obtained from the calibration exposures (solid line). Dashed line represents distribution expected from nuclear interactions.

Fig. 12. Electron energy spectra recorded at the balloon before correction for atmospheric secondaries or energy loss in the atmosphere. The depth of Flight 1195 was 2.0 g/cm^2 while that of Flight 1058 was 8.3 g/cm^2. Squares and circles refer, respectively, to data before and after correction for the selection effects whose probabilities are given in Figure 7.

Fig. 13. Electron energy spectra corrected to the top of the atmosphere. The overall agreement among three flights indicates that corrections appropriate to electrons serve to remove the instrumental and atmospheric effects exhibited in Figure 12.

Fig. 14. Spectral intensity multiplied by E^3 for electrons observed in the present experiment compared with existing data above 50 GeV indicates spectral indicies ranging from 3.0 (dashed line) through 3.3 (solid line) suggested by this experiment to a maximum of 3.5 suggested by Nishimura, et al. (1969).

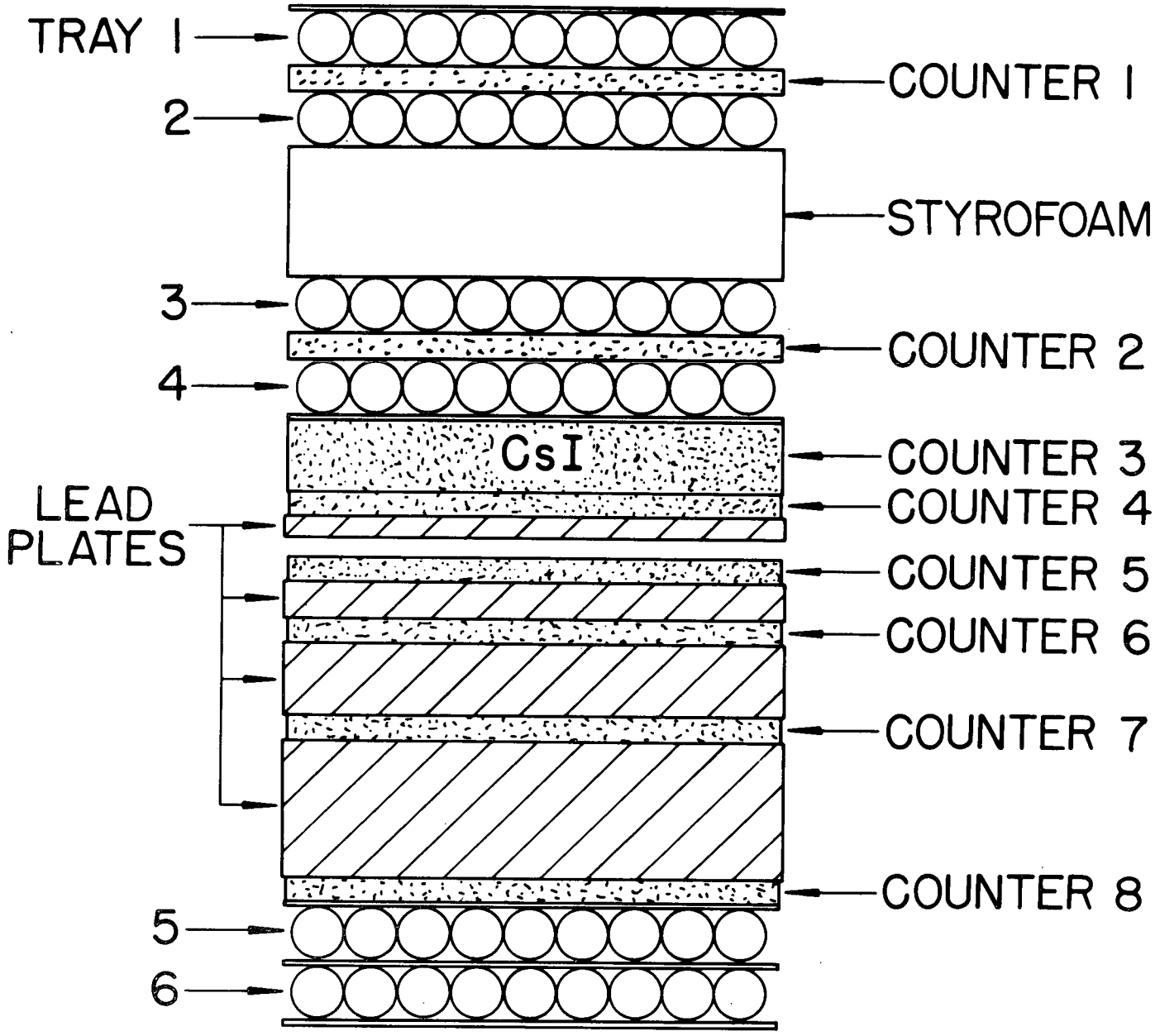
TRAY 1
2
3
4
LEAD PLATES
5
6
CsI
COUNTER 1
STYROFOAM
COUNTER 2
COUNTER 3
COUNTER 4
COUNTER 5
COUNTER 6
COUNTER 7
COUNTER 8

Figure 1

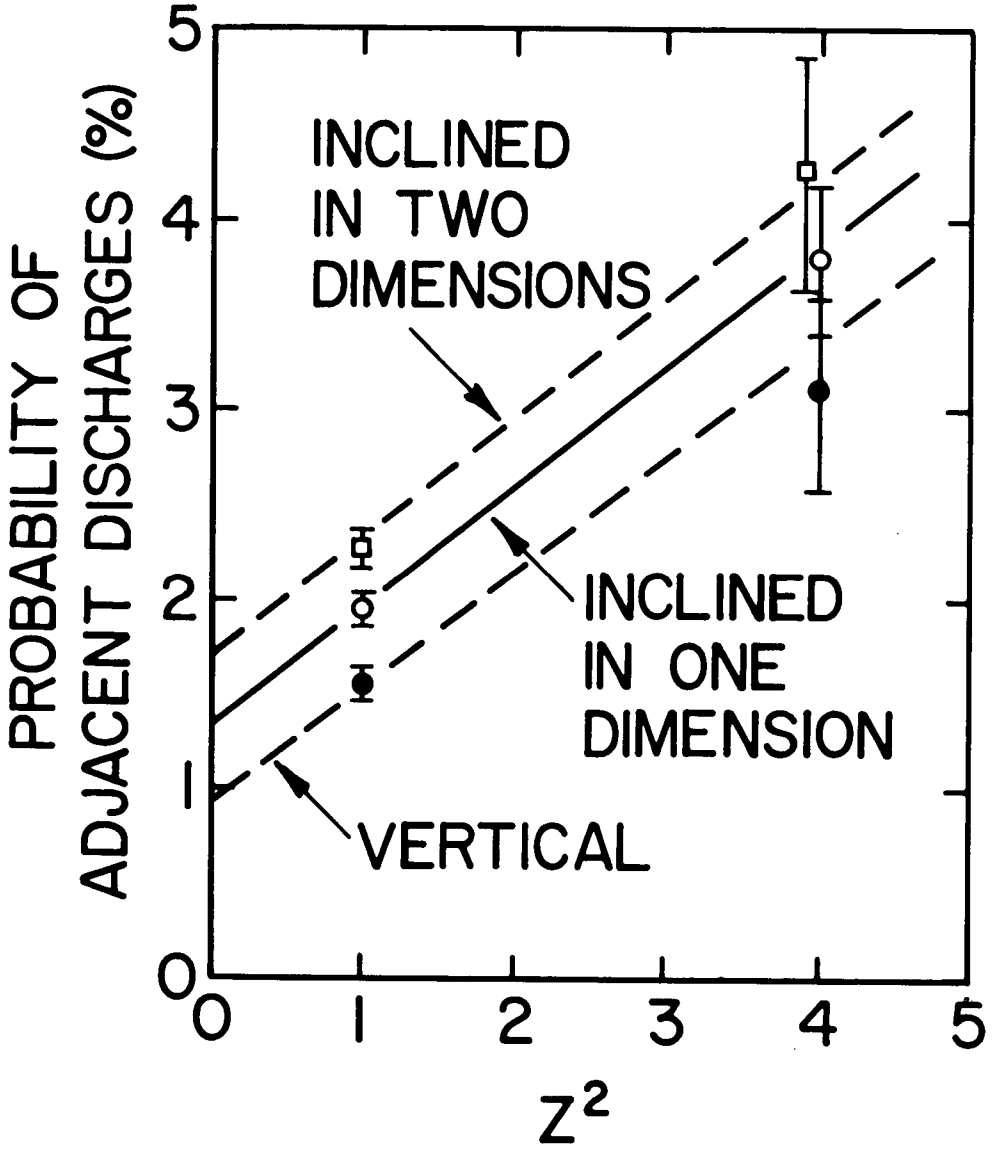
PROBABILITY OF ADJACENT DISCHARGES (%)
INCLINED IN TWO DIMENSIONS
INCLINED IN ONE DIMENSION
VERTICAL
0
1
2
3
4
5
Z^2

Figure 2

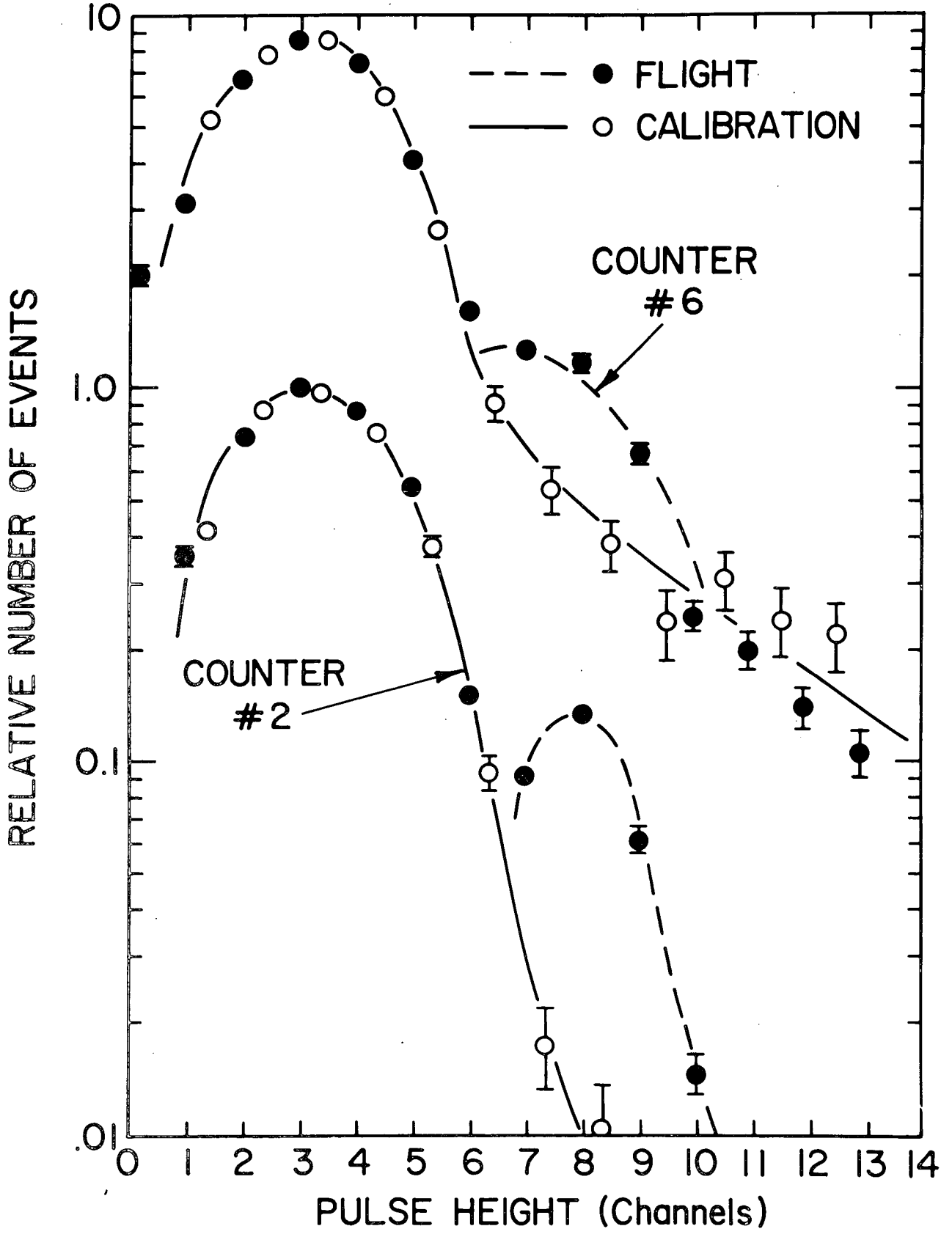
10
1.0
0.1
.01
RELATIVE NUMBER OF EVENTS
FLIGHT
CALIBRATION
COUNTER
#6
COUNTER
#2
0 1 2 3 4 5 6 7 8 9 10 11 12 13 14
PULSE HEIGHT (Channels)

Figure 3

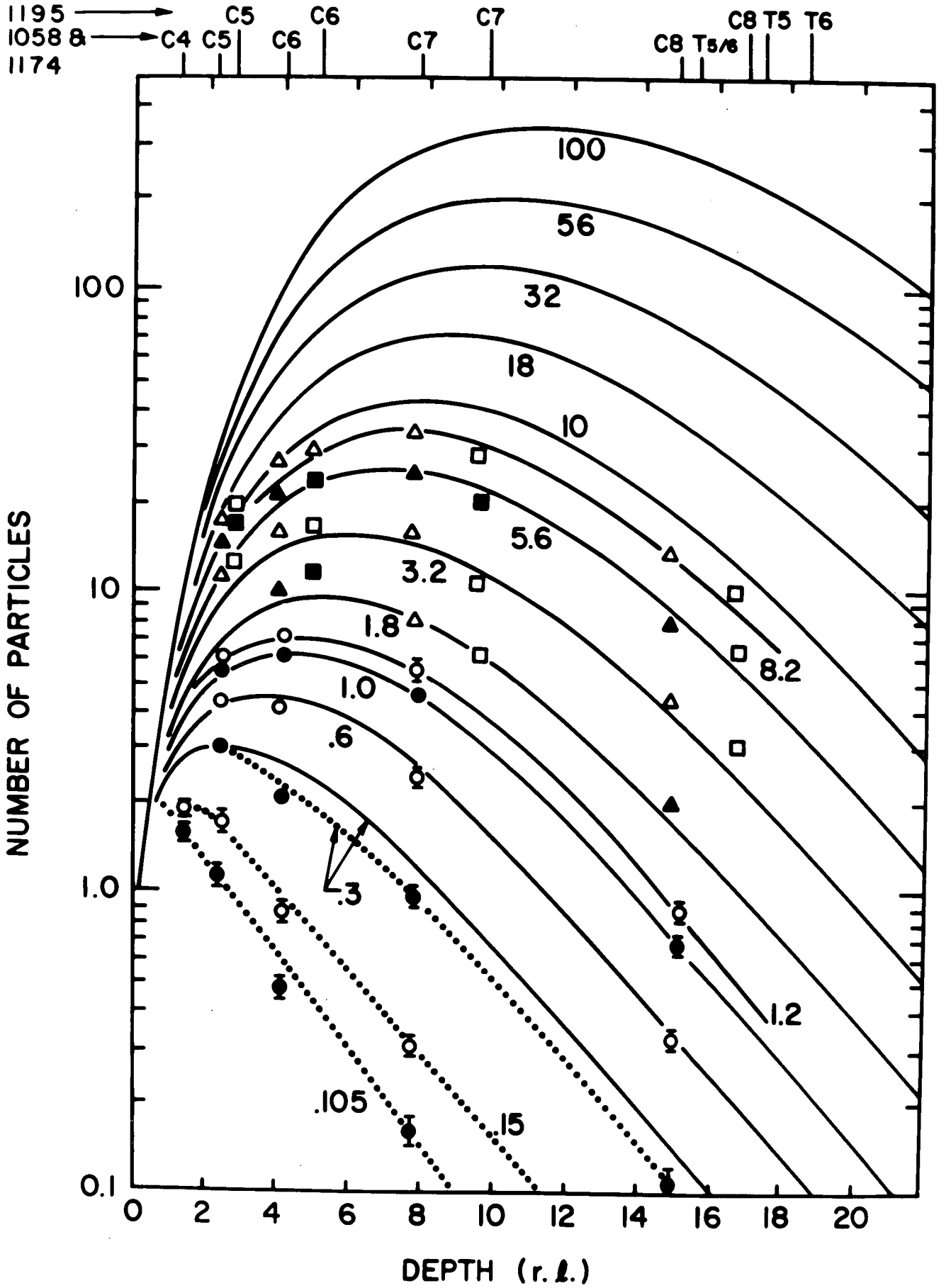
1195
1058 &
1174
C4
C5
C5
C6
C6
C7
C7
C8
C8
T5/6
T5
T6
100
56
32
18
10
5.6
3.2
1.8
1.0
.6
.3
.15
.105
8.2
1.2
NUMBER OF PARTICLES
100
10
1.0
0.1
0
2
4
6
8
10
12
14
16
18
20
DEPTH (r.l.)

Figure 4

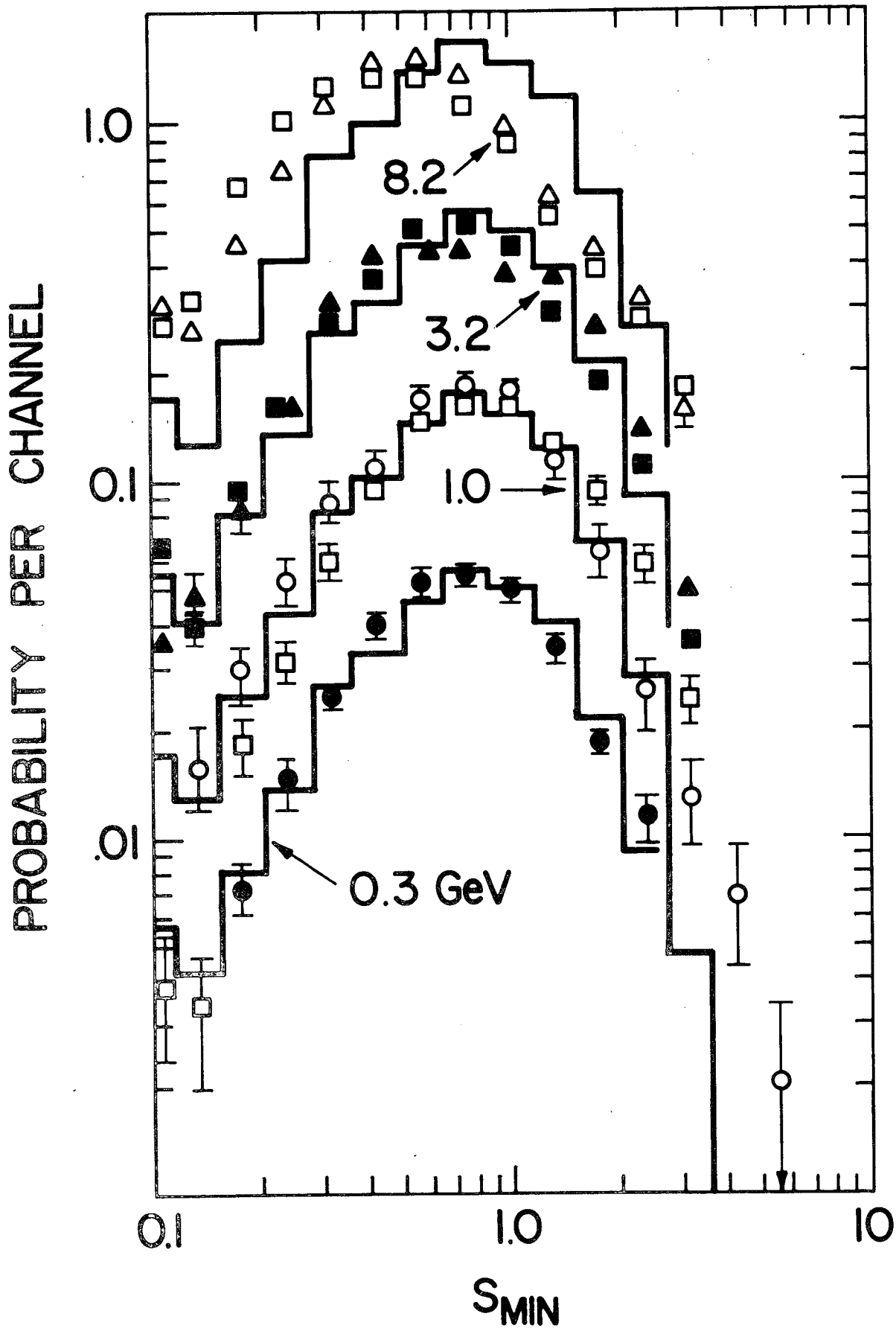

Figure 5

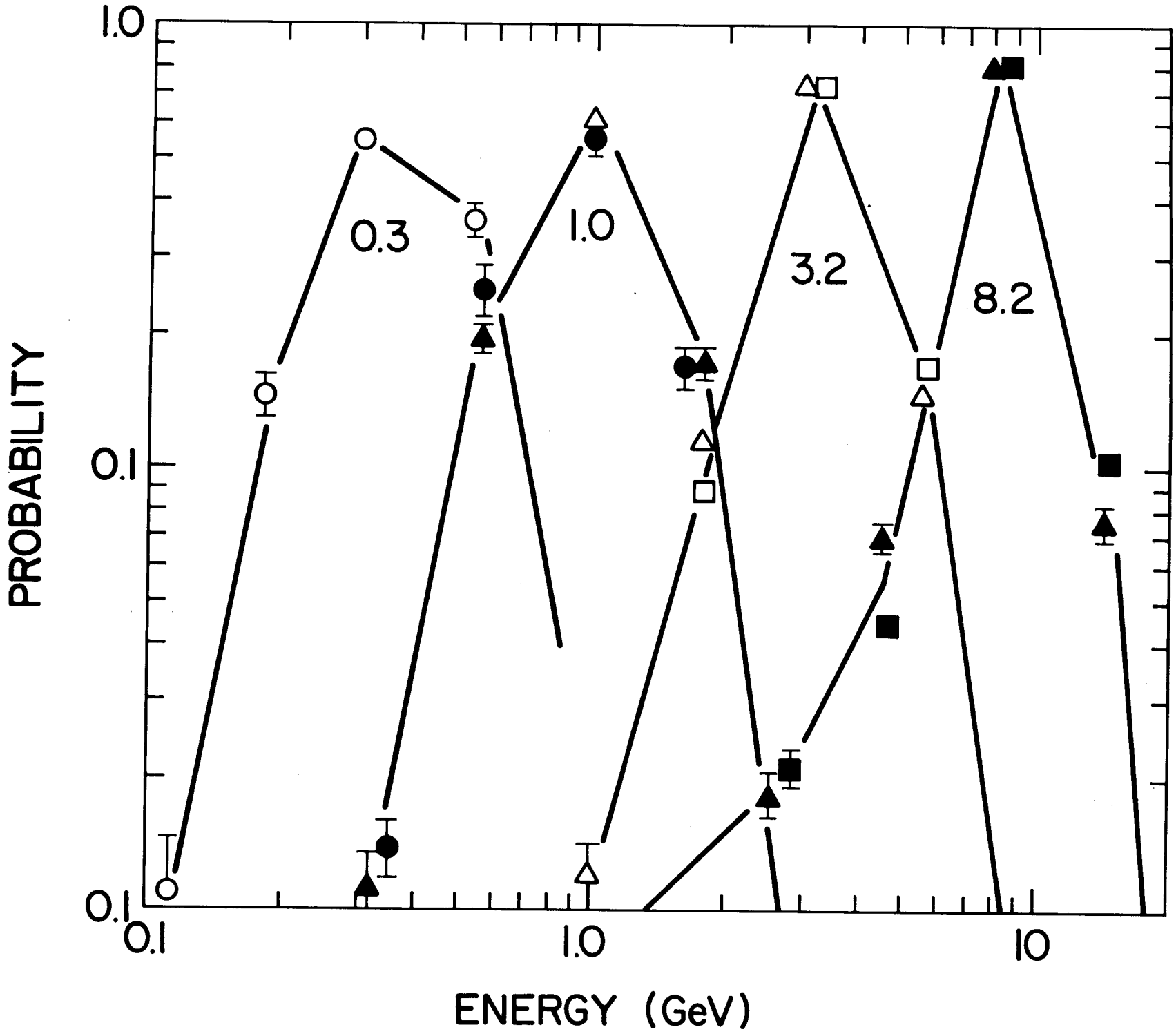

Figure 6

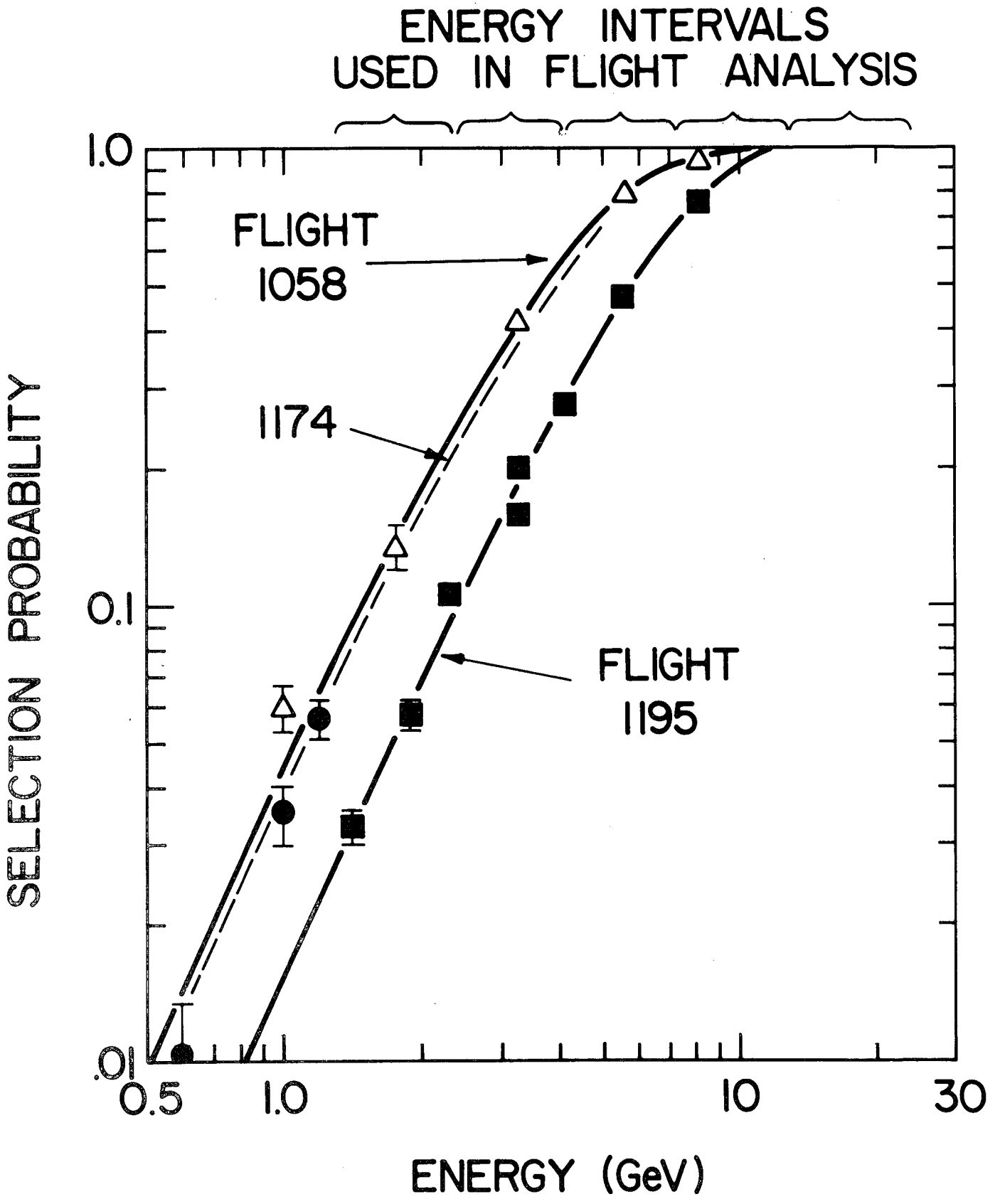
ENERGY INTERVALS
USED IN FLIGHT ANALYSIS
1.0
0.1
.01
SELECTION PROBABILITY
FLIGHT
1058
1174
FLIGHT
1195
0.5
1.0
10
30
ENERGY (GeV)

Figure 7

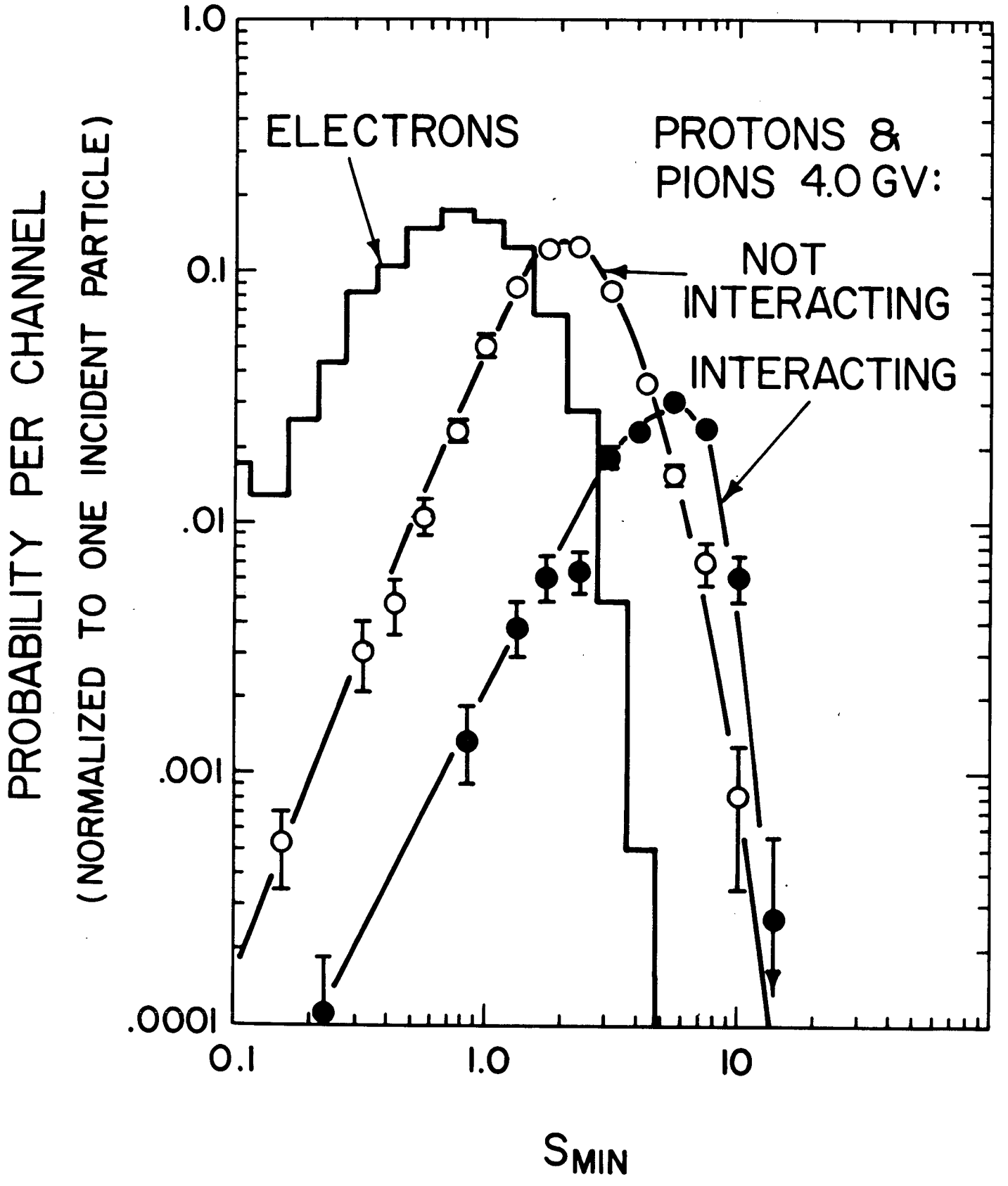
1.0
0.1
.01
.001
.0001
0.1
1.0
10
ELECTRONS
PROTONS &
PIONS 4.0 GV:
NOT
INTERACTING
INTERACTING
PROBABILITY PER CHANNEL
(NORMALIZED TO ONE INCIDENT PARTICLE)
SMIN

Figure 8

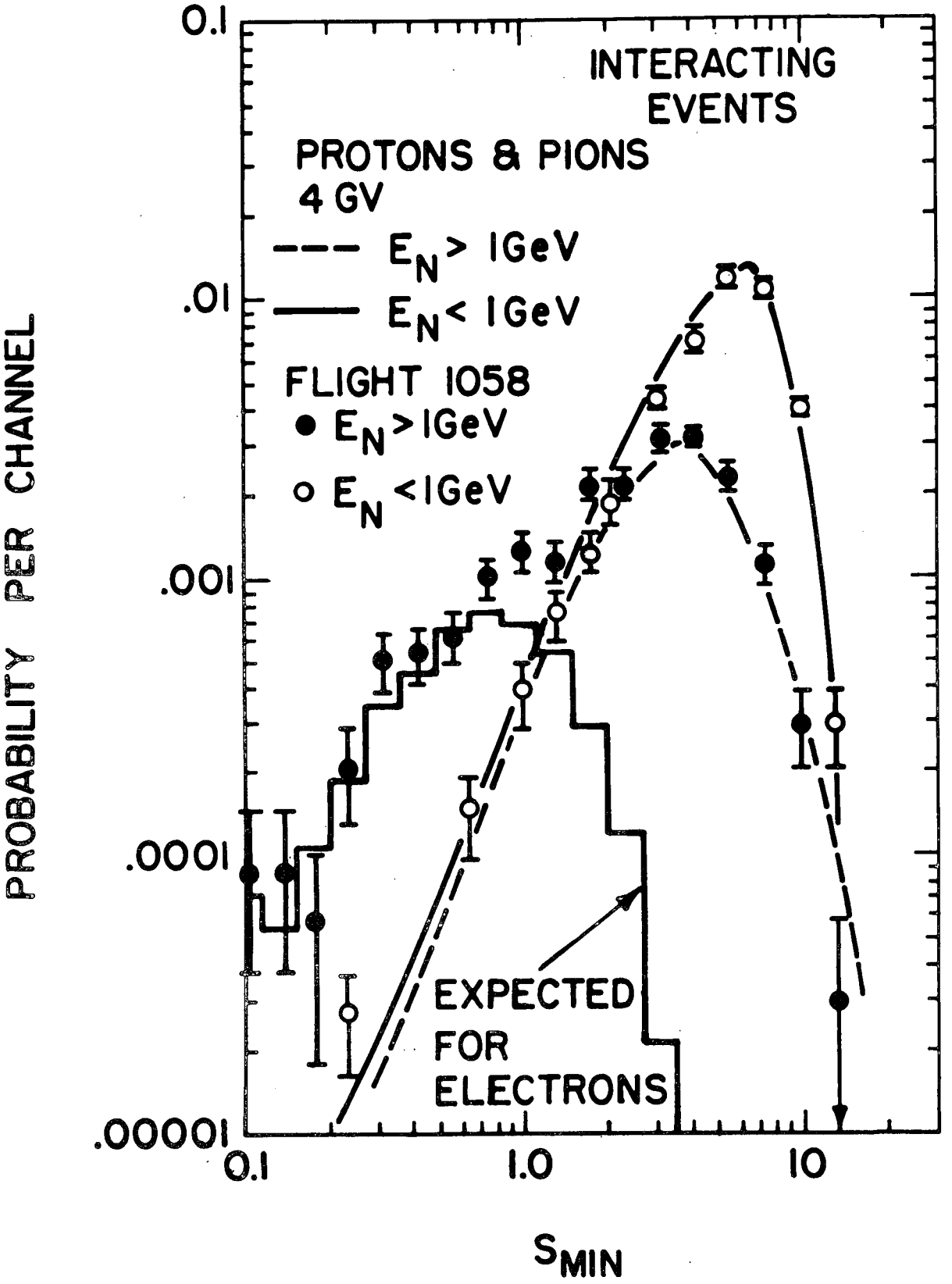
INTERACTING
EVENTS
PROTONS & PIONS
4 GV
--- E_N > 1GeV
—— E_N < 1GeV
FLIGHT 1058
● E_N > 1GeV
○ E_N < 1GeV
EXPECTED
FOR
ELECTRONS
PROBABILITY PER CHANNEL
0.1
.01
.001
.0001
.00001
0.1
1.0
10
S_{MIN}

Figure 9

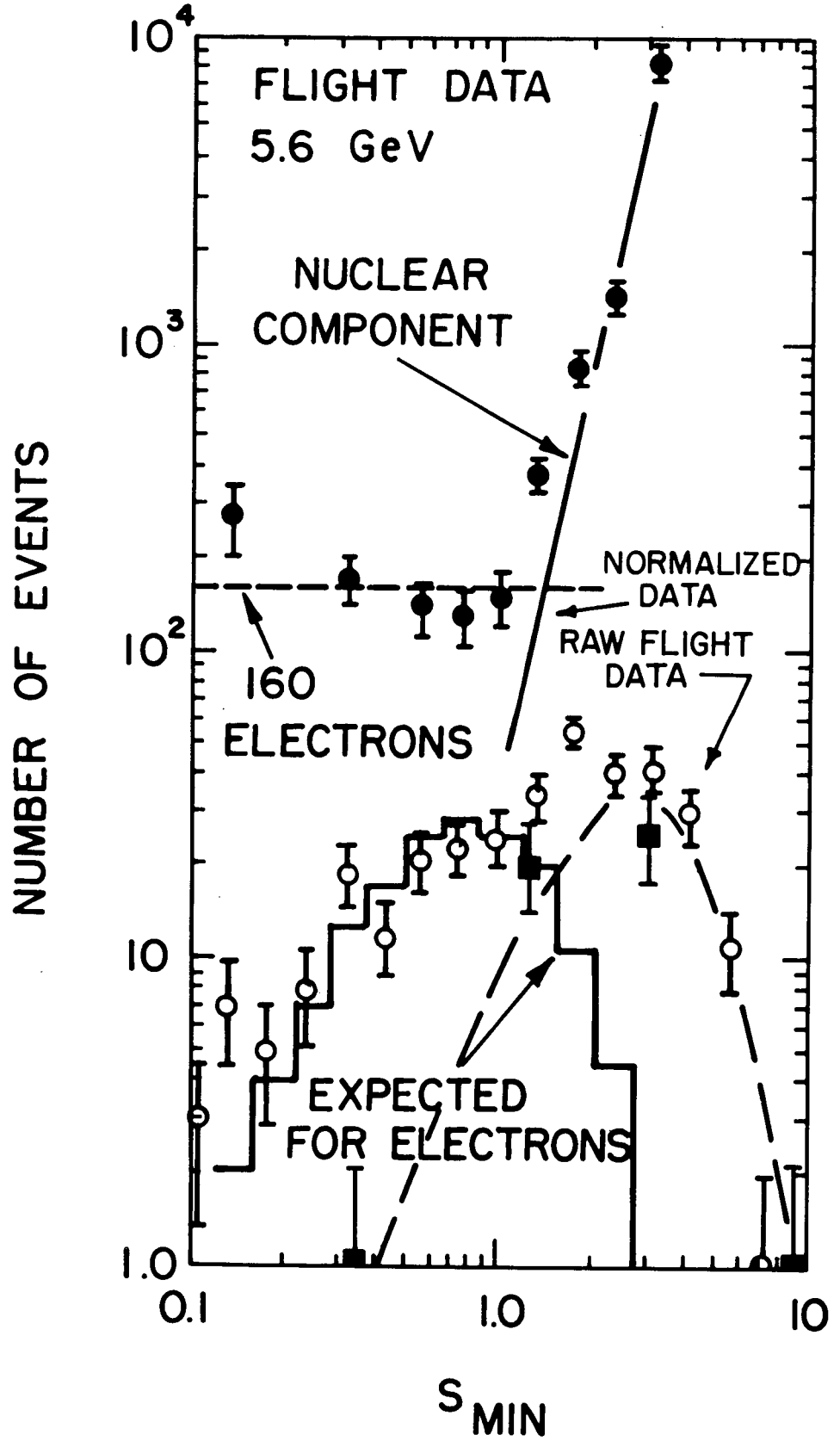
FLIGHT DATA
5.6 GeV
NUCLEAR
COMPONENT
NORMALIZED
DATA
RAW FLIGHT
DATA
160
ELECTRONS
EXPECTED
FOR ELECTRONS
NUMBER OF EVENTS
10^4
10^3
10^2
10
1.0
0.1
1.0
10
S_{MIN}

Figure 10

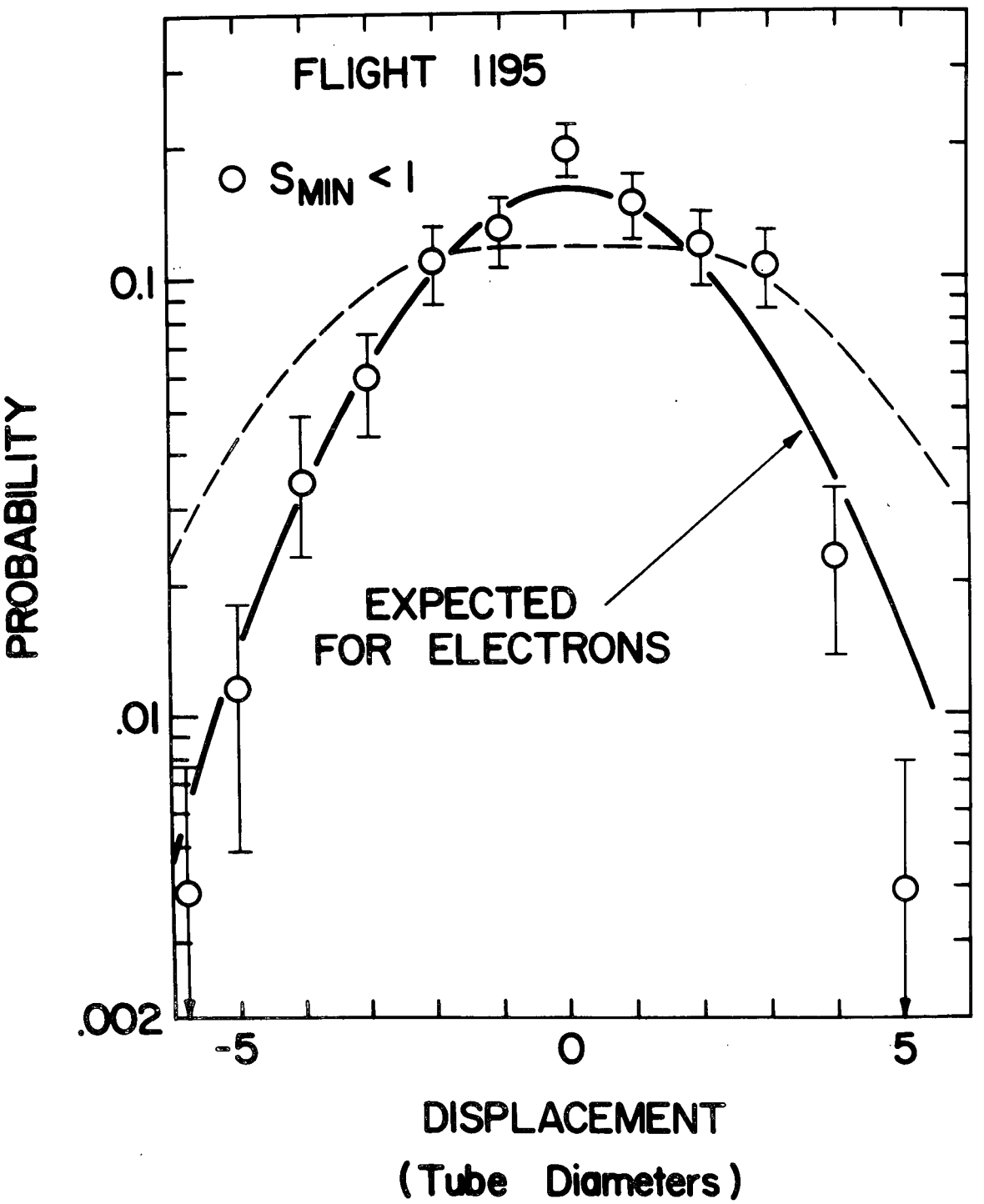
FLIGHT 1195
○ $S_{MIN} < 1$
0.1
.01
.002
PROBABILITY
EXPECTED
FOR ELECTRONS
-5
0
5
DISPLACEMENT
(Tube Diameters)

Figure 11

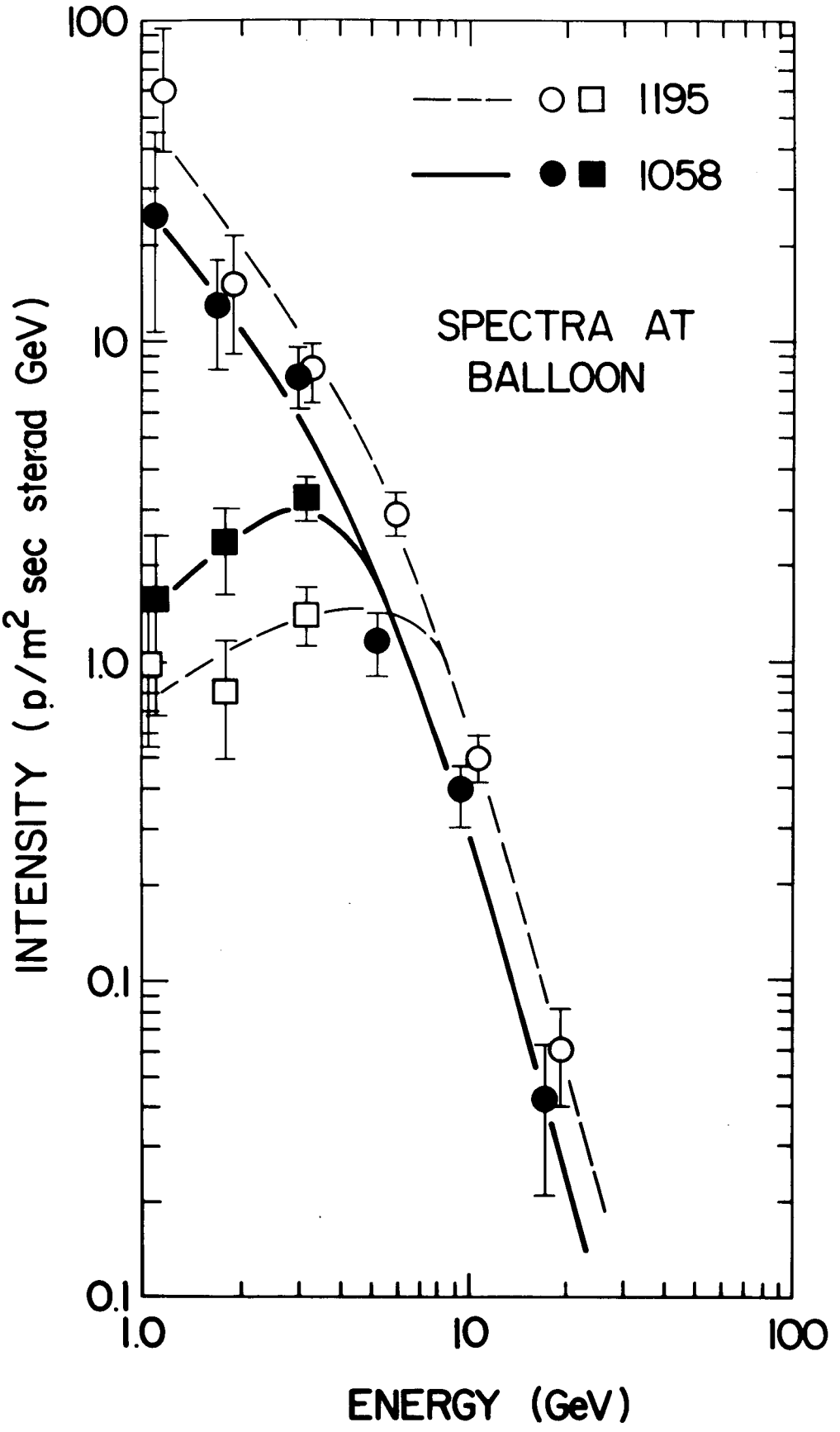
100
10
1.0
0.1
0.1
1.0
10
100
INTENSITY (p/m² sec sterad GeV)
ENERGY (GeV)
1195
1058
SPECTRA AT
BALLOON

Figure 12

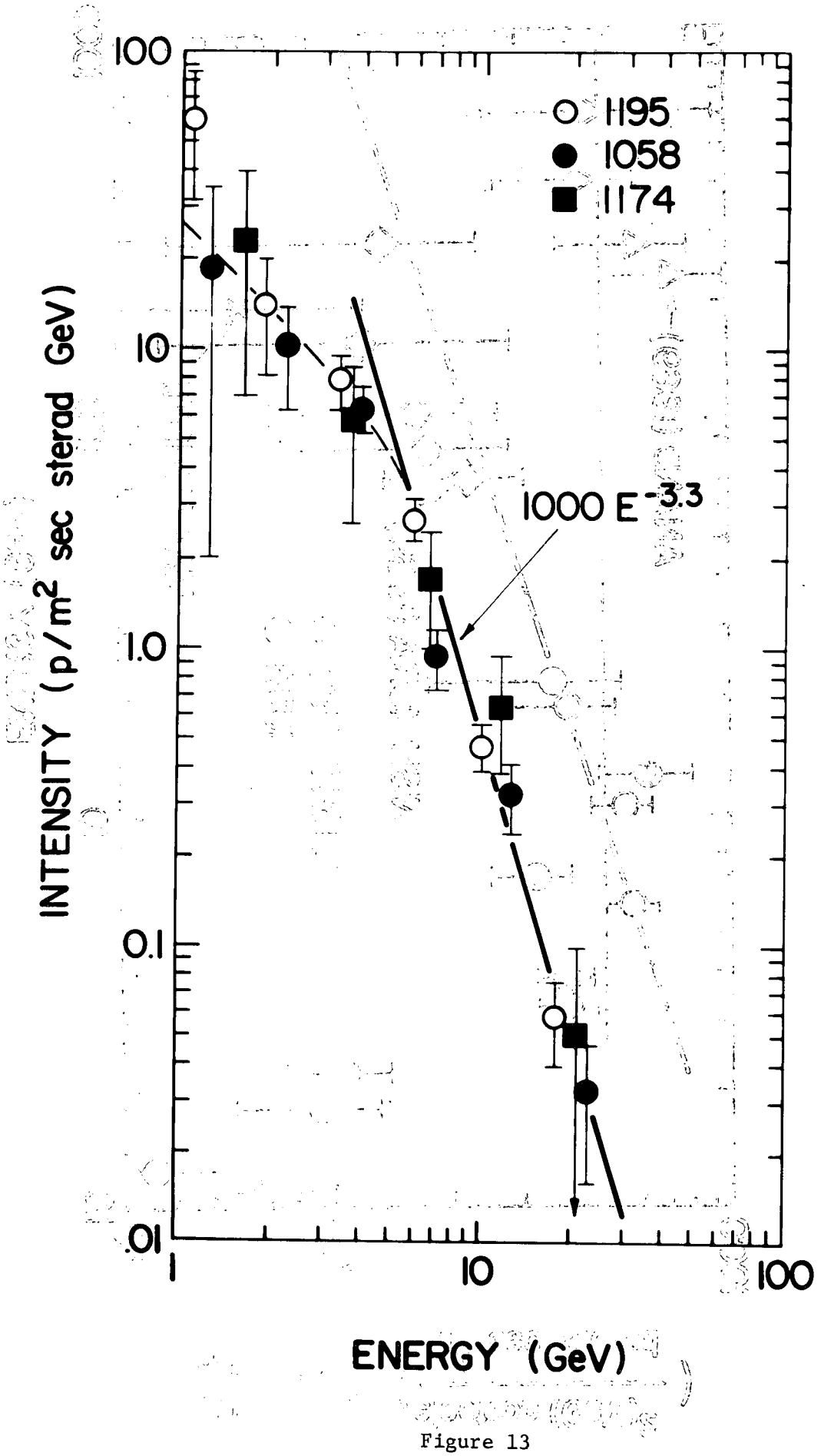
100
10
1.0
0.1
.01
1
10
100
1195
1058
1174
1000 E^-3.3
INTENSITY (p/m² sec sterad GeV)
ENERGY (GeV)

Figure 13

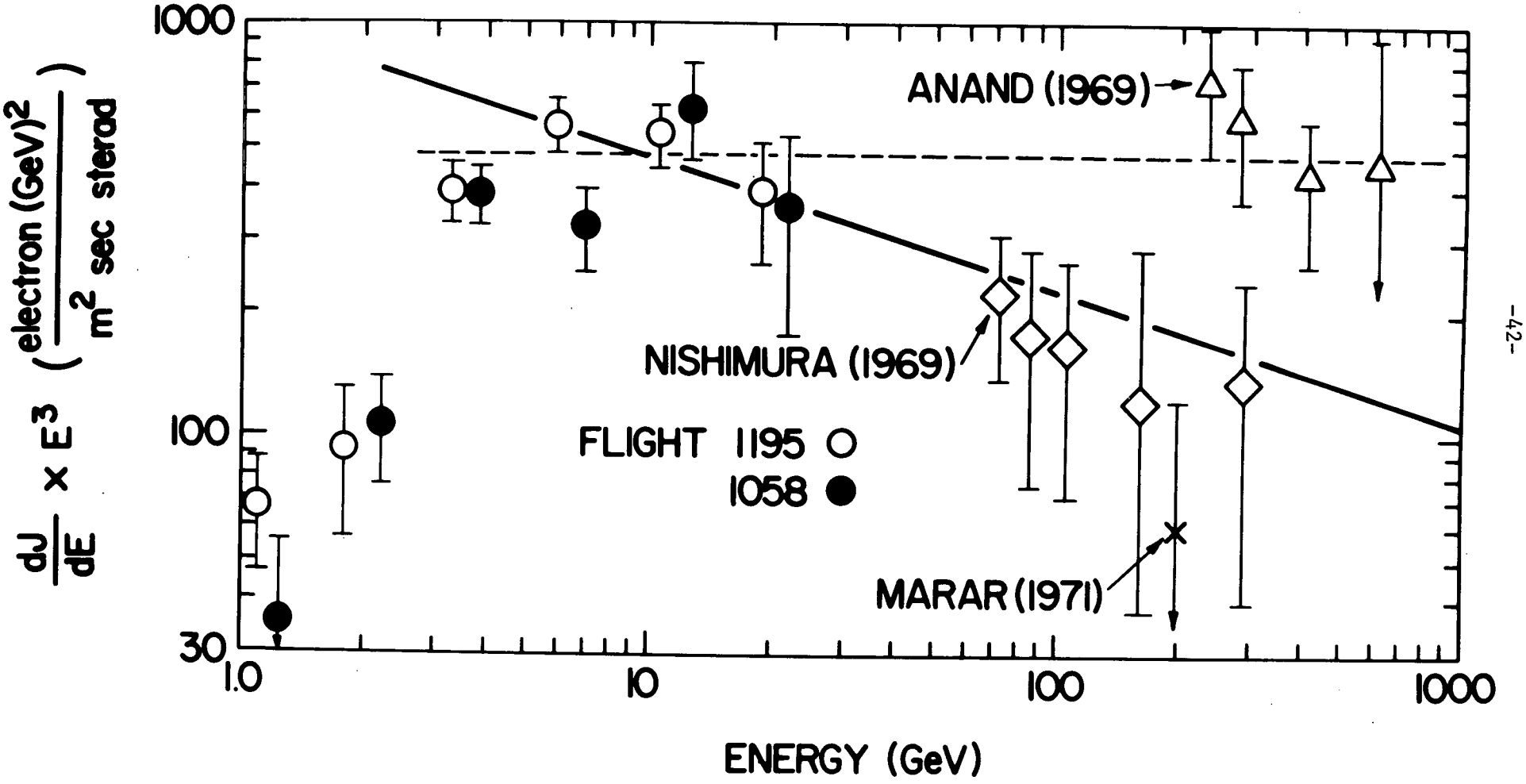
1000
100
30
1.0
10
100
1000
ANAND (1969)
NISHIMURA (1969)
FLIGHT 1195 ○
1058 ●
MARAR (1971)
ENERGY (GeV)
dJ/dE × E³ (electron (GeV)²/m² sec sterad)

Figure 14